



Measurement of $\gamma\gamma \rightarrow p\bar{p}$ production at Belle

Belle Collaboration

C. C. Kuo^u, K. Abe^f, I. Adachi^f, H. Aihara^{ao}, Y. Asano^{as},
V. Aulchenko^a, T. Aushev^j, S. Bahinipati^d, A. M. Bakich^{aj},
A. Bay^o, I. Bedny^a, U. Bitenc^k, I. Bizjak^k, S. Blyth^w,
A. Bondar^a, A. Bozek^x, M. Bračko^{f,q,k}, M.-C. Chang^w,
P. Chang^w, A. Chen^u, W. T. Chen^u, B. G. Cheon^c,
R. Chistov^j, Y. Choi^{ai}, A. Chuvikov^{ae}, S. Cole^{aj}, J. Dalseno^r,
M. Danilov^j, M. Dash^{at}, A. Drutskoy^d, S. Eidelman^a,
Y. Enari^s, S. Fratina^k, N. Gabyshev^a, T. Gershon^f, A. Go^u,
G. Gokhroo^{ak}, A. Gorišek^k, J. Haba^f, K. Hayasaka^s,
H. Hayashii^t, M. Hazumi^f, T. Hokuue^s, Y. Hoshi^{am}, S. Hou^u,
W.-S. Hou^w, T. Iijima^s, A. Imoto^t, K. Inami^s, A. Ishikawa^f,
R. Itoh^f, M. Iwasaki^{ao}, J. H. Kang^{au}, J. S. Kang^m,
P. Kapusta^x, H. Kawai^b, T. Kawasaki^z, H. R. Khan^{ap},
H. Kichimi^f, H. J. Kimⁿ, S. M. Kim^{ai}, P. Krokovny^a,
R. Kulasiri^d, S. Kumar^{ac}, A. Kuzmin^a, Y.-J. Kwon^{au},
G. Lederⁱ, T. Lesiak^x, S.-W. Lin^w, D. Liventsev^j,
J. MacNaughtonⁱ, G. Majumder^{ak}, F. Mandlⁱ,
T. Matsumoto^{aq}, A. Matyja^x, W. Mitaroffⁱ, H. Miyake^{ab},
R. Mizuk^j, G. R. Moloney^r, T. Mori^{ap}, Y. Nagasaka^g,
E. Nakano^{aa}, M. Nakao^f, H. Nakazawa^f, Z. Natkaniec^x,
S. Nishida^f, O. Nitoh^{ar}, S. Ogawa^{al}, T. Ohshima^s, S. Okuno^l,
S. L. Olsen^e, W. Ostrowicz^x, H. Palka^x, H. Parkⁿ,
L. S. Peak^{aj}, R. Pestotnik^k, L. E. Piilonen^{at}, A. Poluektov^a,
H. Sagawa^f, Y. Sakai^f, N. Sato^s, T. Schietinger^o,
O. Schneider^o, K. Senyo^s, M. E. Sevier^r, H. Shibuya^{al},
B. Shwartz^a, J. B. Singh^{ac}, A. Somov^d, N. Soni^{ac}, R. Stamen^f,
S. Stanič^{as,1}, M. Starič^k, A. Sugiyama^{af}, T. Sumiyoshi^{aq},

S. Y. Suzuki^f, O. Tajima^f, F. Takasaki^f, K. Tamai^f,
N. Tamura^z, G. N. Taylor^r, Y. Teramoto^{aa}, X. C. Tian^{ad},
T. Tsukamoto^f, S. Uehara^f, K. Ueno^w, T. Uglov^j, S. Uno^f,
G. Varner^e, S. Villa^o, C. C. Wang^w, C. H. Wang^v,
M. Watanabe^z, Q. L. Xie^h, B. D. Yabsley^{at}, A. Yamaguchi^{an},
Y. Yamashita^y, M. Yamauchi^f, Heyoung Yang^{ah}, J. Ying^{ad},
L. M. Zhang^{ag}, Z. P. Zhang^{ag}, V. Zhilich^a, D. Žontar^{p,k} and
D. Zürcher^o

^a*Budker Institute of Nuclear Physics, Novosibirsk, Russia*

^b*Chiba University, Chiba, Japan*

^c*Chonnam National University, Kwangju, South Korea*

^d*University of Cincinnati, Cincinnati, OH, USA*

^e*University of Hawaii, Honolulu, HI, USA*

^f*High Energy Accelerator Research Organization (KEK), Tsukuba, Japan*

^g*Hiroshima Institute of Technology, Hiroshima, Japan*

^h*Institute of High Energy Physics, Chinese Academy of Sciences, Beijing, PR
China*

ⁱ*Institute of High Energy Physics, Vienna, Austria*

^j*Institute for Theoretical and Experimental Physics, Moscow, Russia*

^k*J. Stefan Institute, Ljubljana, Slovenia*

^l*Kanagawa University, Yokohama, Japan*

^m*Korea University, Seoul, South Korea*

ⁿ*Kyungpook National University, Taegu, South Korea*

^o*Swiss Federal Institute of Technology of Lausanne, EPFL, Lausanne, Switzerland*

^p*University of Ljubljana, Ljubljana, Slovenia*

^q*University of Maribor, Maribor, Slovenia*

^r*University of Melbourne, Victoria, Australia*

^s*Nagoya University, Nagoya, Japan*

^t*Nara Women's University, Nara, Japan*

^u*National Central University, Chung-li, Taiwan*

^v*National United University, Miao Li, Taiwan*

^w*Department of Physics, National Taiwan University, Taipei, Taiwan*

^x*H. Niewodniczanski Institute of Nuclear Physics, Krakow, Poland*

^y*Nihon Dental College, Niigata, Japan*

^z*Niigata University, Niigata, Japan*

^{aa}*Osaka City University, Osaka, Japan*

- ^{ab} *Osaka University, Osaka, Japan*
^{ac} *Panjab University, Chandigarh, India*
^{ad} *Peking University, Beijing, PR China*
^{ae} *Princeton University, Princeton, NJ, USA*
^{af} *Saga University, Saga, Japan*
^{ag} *University of Science and Technology of China, Hefei, PR China*
^{ah} *Seoul National University, Seoul, South Korea*
^{ai} *Sungkyunkwan University, Suwon, South Korea*
^{aj} *University of Sydney, Sydney, NSW, Australia*
^{ak} *Tata Institute of Fundamental Research, Bombay, India*
^{al} *Toho University, Funabashi, Japan*
^{am} *Tohoku Gakuin University, Tagajo, Japan*
^{an} *Tohoku University, Sendai, Japan*
^{ao} *Department of Physics, University of Tokyo, Tokyo, Japan*
^{ap} *Tokyo Institute of Technology, Tokyo, Japan*
^{aq} *Tokyo Metropolitan University, Tokyo, Japan*
^{ar} *Tokyo University of Agriculture and Technology, Tokyo, Japan*
^{as} *University of Tsukuba, Tsukuba, Japan*
^{at} *Virginia Polytechnic Institute and State University, Blacksburg, VA, USA*
^{au} *Yonsei University, Seoul, South Korea*

Abstract

A high precision study of the process $\gamma\gamma \rightarrow p\bar{p}$ has been performed using a data sample of 89 fb^{-1} collected with the Belle detector at the KEKB e^+e^- collider. The cross section of $p\bar{p}$ production has been measured at two-photon center-of-mass (c.m.) energies between 2.025 and 4.0 GeV and in the c.m. angular range of $|\cos\theta^*| < 0.6$. Production of $\gamma\gamma \rightarrow \eta_c \rightarrow p\bar{p}$ is observed and the product of the two-photon width of the η_c and its branching ratio to $p\bar{p}$ is determined.

PACS numbers: 12.38.Qk, 13.60.Rj, 14.40.Gx

¹ on leave from Nova Gorica Polytechnic, Nova Gorica, Slovenia

1 Introduction

Two-photon collisions provide a clean environment for baryon pair production and such events can be produced in great abundance at a high luminosity electron-positron collider. Accurate measurements of such processes, in particular $\gamma\gamma \rightarrow p\bar{p}$, is important to test existing theoretical predictions.

General theories of hard exclusive processes in QCD [1,2] (see also [3] for a review) predict that the differential cross section for $\gamma\gamma \rightarrow h_1 h_2$ at large energies and fixed c.m. angle (θ^*) has the form

$$d\sigma/dt \propto s^{2-n_c} f(\theta^*) \quad (\text{as } s \rightarrow \infty). \quad (1)$$

Here n_c is the number of elementary constituents participating in the hard interaction, $f(\theta^*)$ is a specific function expressed via definite integrals over hadron wave functions, s is the square of the c.m. energy of the two-photon system, and t is the square of the four-momentum transfer from a photon to hadron. The first estimate of the cross section for $\gamma\gamma \rightarrow p\bar{p}$ was obtained in the three-quark picture ($n_c = 8$) [4,5], using the proton wave function based on QCD sum rules [6]. Previous measurements [7,8,9,10,11] in the $W_{\gamma\gamma} (\equiv \sqrt{s})$ range between 2.5 and 3.0 GeV gave cross sections one order of magnitude larger than this expectation. To explain these experimental observations, various model-dependent approaches were suggested. For example, in the diquark model [12,13,14] the proton is considered to be a quark-diquark system. In this case $n_c = 6$ and a diquark form factor is introduced, so that Eq. (1) becomes $d\sigma/dt \propto s^{-4}|F|^2$, where F may depend on s . Asymptotically, $F \rightarrow f(\theta^*)/s$ [12], and the behavior $d\sigma/dt \propto s^{-6}$ is recovered. These results exhibit better agreement with measurements of the absolute size of the cross section for $W_{\gamma\gamma} = 2.5 - 3.0$ GeV.

Other approaches have been developed recently. The handbag model [15] has been developed for large momentum transfers, and the calculations have been applied at medium energies ($W_{\gamma\gamma} > 2.55$ GeV) with large uncertainty bands. In Ref. [16], the Veneziano model is applied in an unmodified form to the process, and fair agreement with data is obtained without adjustable parameters.

Recently, the measured energy range for $\gamma\gamma \rightarrow p\bar{p}$ has been extended to $W_{\gamma\gamma} = 4$ GeV and above [10,11], but with very limited statistics for $W_{\gamma\gamma} > 3$ GeV. Furthermore, $p\bar{p} \rightarrow \gamma\gamma$ experiments give the cross section for the inverse process at $W_{\gamma\gamma} = 3.2 - 3.7$ GeV [17]. To test QCD predictions, it is very important to improve the statistics at higher energies. Moreover, an accurate measurement with higher statistics for $\gamma\gamma \rightarrow p\bar{p}$ is crucial in the study of the interactions involved. This paper presents the Belle measurement of the $\gamma\gamma \rightarrow p\bar{p}$ cross section for $W_{\gamma\gamma}$ between 2.025 to 4.0 GeV and $|\cos\theta^*| < 0.6$,

using a data sample corresponding to an integrated luminosity of 89 fb^{-1} .

2 Experimental apparatus and event selection

Experimental data are recorded with the Belle detector [18] at KEKB [19], which is an asymmetric e^+e^- collider running at 10.58 GeV c.m. energy. In the laboratory frame, the direction of the positron beam is taken to define the $-z$ direction. For the analyses in this paper, the following Belle subsystems are of importance: the central drift chamber (CDC), the aerogel Cherenkov counters (ACC), the time-of-flight scintillation counters (TOF) and the CsI electromagnetic calorimeter (ECL), all of which are located in a 1.5 T solenoidal magnetic field. The CDC measures the momenta of charged particles and provides particle identification information by precise (6%) dE/dx measurement, allowing separation of protons from other particles for momentum up to 1 GeV/ c . The TOF measures the time of flight of particles with a 0.1 ns timing resolution, which is powerful for p/K separation for momentum up to 2 GeV/ c . The ECL detects photons and is used to reject electrons by measuring the deposited energy with a resolution of $\sigma_E/E = 1.5\%$ (2.0%) at 1 GeV (0.1 GeV). Using the number of photoelectrons observed, the ACC extends particle identification beyond that of the CDC dE/dx and TOF and is effective in the suppression of highly relativistic π^\pm, μ^\pm and e^\pm up to a momentum of 3.5 GeV/ c .

Through the process $e^+e^- \rightarrow e^+e^-\gamma^*\gamma^* \rightarrow e^+e^-p\bar{p}$, exclusive $p\bar{p}$ pairs are produced in quasi-real two-photon collisions, where the scattered e^+ and e^- are lost down the beam-pipe, and only the p and \bar{p} can be detected. The $\gamma\gamma$ axis thus approximates the beam direction in the e^+e^- c.m. frame. Candidate events are searched for in a data stream where the sum of the magnitudes of momentum of all charged tracks and the total ECL energy are restricted to 6 GeV/ c and 6 GeV, respectively. Events are required to have exactly two tracks of opposite charge satisfying the following conditions in the laboratory frame: $p_t > 0.35 \text{ GeV}/c$, $dr < 1 \text{ cm}$ and $|dz| < 5 \text{ cm}$. Here p_t is the transverse momentum and dr and dz are the radial and axial coordinates of the point of closest approach to the nominal collision point, respectively. Both tracks are required to hit the TOF counters. The invariant mass of the two tracks and the squared missing mass of the event, assuming the two tracks are massless, are required to be smaller than $4.5 \text{ GeV}/c^2$ and larger than $2 \text{ GeV}^2/c^4$, respectively. A good transverse momentum balance in the e^+e^- c.m. frame is also required: $|\Sigma p_t^*| \equiv |\vec{p}_{t_1}^* + \vec{p}_{t_2}^*| < 0.2 \text{ GeV}/c$, where $\vec{p}_{t_1}^*$ and $\vec{p}_{t_2}^*$ denote the transverse momenta of the two tracks in that frame, with respect to the e^+e^- beam-axis.

The selected events are dominated by $\gamma\gamma \rightarrow e^+e^-, \mu^+\mu^-, \pi^+\pi^-$ and K^+K^- up to this stage. Events with $p\bar{p}$ are separated from the others by a particle iden-

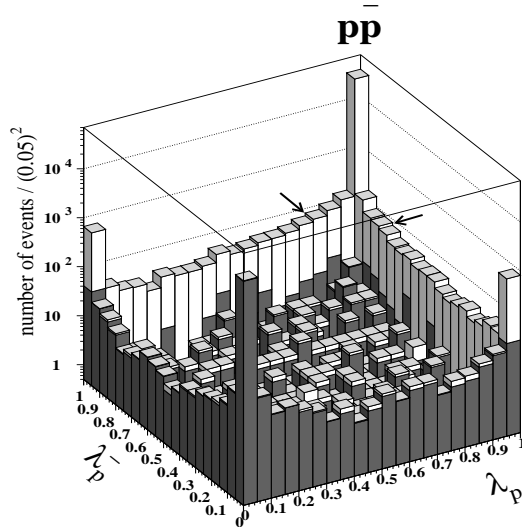


Fig. 1. Two-dimensional distribution of the normalized likelihood for $p\bar{p}$ identification, for the events passing all selection criteria except the cuts on the normalized likelihood indicated by the arrows. The dark parts show the events satisfying $\lambda_x \equiv L_x / (L_p + L_K + L_\pi + L_\mu + L_e) > 0.01$ for both tracks using the same x , where x is K , π , μ or e .

tification (PID) algorithm, which is applied to each individual track under the following conditions: 1) the difference between the measured and the expected CDC dE/dx is less than 4 times the resolution: $\chi_{dE/dx}^2 \equiv [\Delta(dE/dx) / \sigma_{dE/dx}]^2 < 4^2$; 2) the ratio of the associated ECL energy to the momentum is less than 0.9, which is only applied to the positively charged track; 3) the number of the photoelectrons in ACC counters associated with the track is less than 4, and this condition removes a large part of high-momentum π^\pm, μ^\pm and e^\pm ; 4) the likelihoods for each particle assignment are combined to determine the normalized likelihood, $\lambda_p \equiv L_p / (L_p + L_K + L_\pi + L_\mu + L_e)$, which has to be larger than 0.8 (Fig. 1). In these likelihoods, $L \equiv \exp[-\frac{1}{2}(\chi_{dE/dx}^2 + \chi_T^2)]$ is calculated using information from the CDC (dE/dx) and the TOF (time of flight T). Here $\chi_T^2 \equiv (\Delta T / \sigma_T)^2$, ΔT is the difference between the measured and the expected values for T , and σ_T is the timing resolution. A combined use of CDC and TOF allows $p(\bar{p})$ separation from other particles, in particular K^\pm , for momentum up to 2 GeV/ c .

For $W_{\gamma\gamma} = 2 - 4$ GeV a total 36094 events survive all of the selection criteria. Their distribution in $W_{\gamma\gamma}$ is shown in Fig. 2. A peak around 2.98 GeV can be identified as the $\eta_c(2980)$ resonance [20]. A much narrower peak at 3.08 - 3.10 GeV, corresponding to an excess of 26 ± 8 events relative to the continuum, could be attributed to backgrounds from radiative return to J/ψ , and the enhancement is in agreement with expectations based on this assumption [21]. Fitting the data from 2.6 to 3.7 GeV with a smooth (exponential of a fifth-order polynomial) function for the continuum, a Breit-Wigner function for the η_c and a Gaussian for the J/ψ , a total η_c yield of 156.9 ± 33.3 events

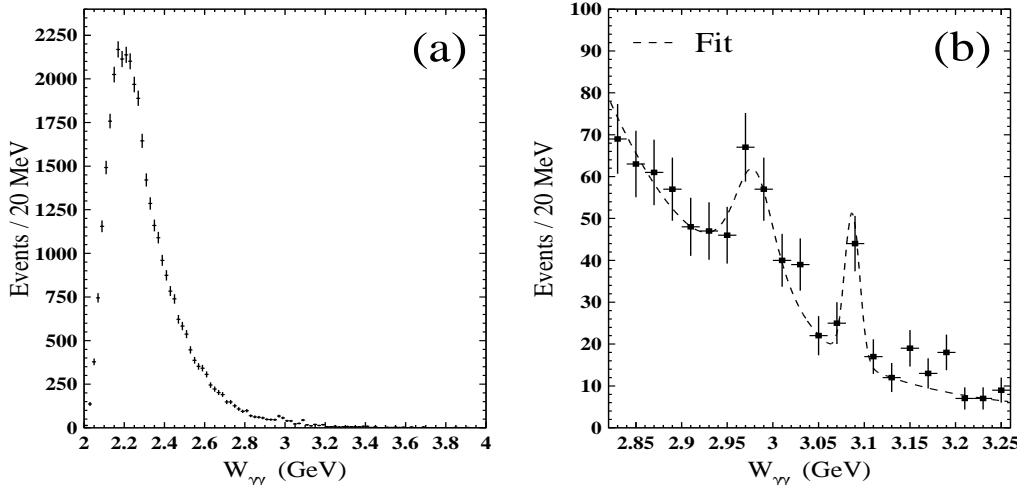


Fig. 2. $W_{\gamma\gamma}$ distribution of events passing all the selection criteria: (a) $W_{\gamma\gamma} = 2 - 4$ GeV; (b) a close-up view of (a) for $W_{\gamma\gamma} = 2.82 - 3.26$ GeV.

is obtained. The statistical significance of the η_c signal is 5.3σ , defined as $\sqrt{-2 \ln(L_0/L_S)}$, where L_S and L_0 denote the maximum likelihoods of the fits with and without a signal component, respectively.

3 Monte Carlo simulation

Monte Carlo samples for the following channels have been generated: $e^+e^- \rightarrow e^+e^-X$ where X is $p\bar{p}$, K^+K^- , $\pi^+\pi^-$, $\mu^+\mu^-$, e^+e^- and $p\bar{p}\pi^0$. Hadron pair, lepton pair and $\gamma\gamma \rightarrow p\bar{p}\pi^0$ events are generated by the codes TREPS [22], AAFH [23] and GGLU [24], respectively. Event generation is followed by a detector simulation based on GEANT3 [25] and a trigger simulation. The selection criteria described in Section 2 are then applied to these Monte Carlo events.

Because the acceptance depends on both $W_{\gamma\gamma}$ and $|\cos\theta^*|$, the signal ($\gamma\gamma \rightarrow p\bar{p}$) efficiencies are determined for a number of two-dimensional bins of the two variables. Other channels are generated for the study of residual backgrounds. Similar to $\gamma\gamma \rightarrow p\bar{p}$, the selection efficiencies for $\gamma\gamma \rightarrow K^+K^-$ and $\gamma\gamma \rightarrow p\bar{p}\pi^0$ are evaluated within each narrow bin. For the $\gamma\gamma \rightarrow \pi^+\pi^-$, $\mu^+\mu^-$ and e^+e^- channels, realistic distributions are generated [23,26,27]. Events from those samples that survive the selection criteria are referred to as the expected residual backgrounds.

From Monte Carlo simulation, the overall efficiency of $\gamma\gamma \rightarrow p\bar{p}$ for $|\cos\theta^*| < 0.1$ ranges from $\sim 3\%$ at $W_{\gamma\gamma} = 2$ GeV to $\sim 32\%$ at $W_{\gamma\gamma} = 4$ GeV (Fig. 3).

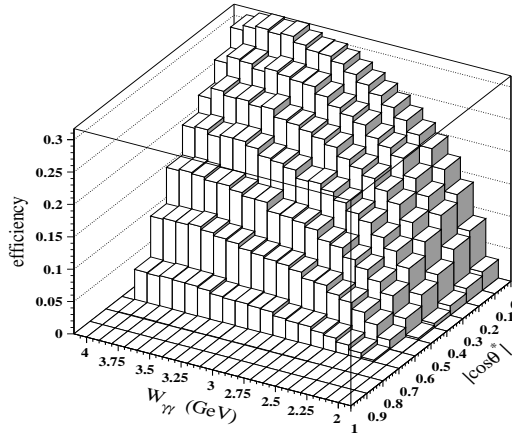


Fig. 3. Overall detection efficiency of $\gamma\gamma \rightarrow p\bar{p}$ as a function of $W_{\gamma\gamma}$ and $|\cos\theta^*|$.

4 Measurement of the cross sections for $\gamma\gamma \rightarrow p\bar{p}$

Dividing $|\cos\theta^*|$ into bins of 0.1, $W_{\gamma\gamma}$ into bins of 25 MeV (for 2 - 3 GeV) and 100 MeV (for 3 - 4 GeV), the number of events selected from the data, $\Delta N(W_{\gamma\gamma}, |\cos\theta^*|)$, is determined for each of the two-dimensional bins. The efficiency $\varepsilon(W_{\gamma\gamma}, |\cos\theta^*|)$ is also evaluated from Monte Carlo simulation for each bin. The ratio of ΔN to ε is then converted to the differential cross section, according to the formula:

$$\frac{d\sigma_{\gamma\gamma \rightarrow p\bar{p}}(W_{\gamma\gamma})}{d|\cos\theta^*|} = \frac{\Delta N(1-f)/\varepsilon}{L_{\text{int}} \frac{dL_{\gamma\gamma}}{dW_{\gamma\gamma}} \Delta W_{\gamma\gamma} \Delta|\cos\theta^*|} \quad (2)$$

where f is the fraction of residual background in the data, L_{int} is the integrated luminosity and $\frac{dL_{\gamma\gamma}}{dW_{\gamma\gamma}}$ is the luminosity function. Here $L_{\text{int}} = 88.96 \text{ fb}^{-1}$, with a systematic uncertainty of 1.4%. The luminosity function $\frac{dL_{\gamma\gamma}}{dW_{\gamma\gamma}}$, as a function of $W_{\gamma\gamma}$, is defined by

$$\sigma_{e^+e^- \rightarrow e^+e^-p\bar{p}} = \int \sigma_{\gamma\gamma \rightarrow p\bar{p}}(W_{\gamma\gamma}) \frac{dL_{\gamma\gamma}(W_{\gamma\gamma})}{dW_{\gamma\gamma}} dW_{\gamma\gamma} \quad (3)$$

and is calculated by TREPS [22] using the equivalent photon approximation method [21]. For the calculation of the luminosity function, the effects from longitudinal photons are neglected. For simulation in TREPS, the maximum virtuality of each of the two photons, Q_1^2 and Q_2^2 , is limited to 1 GeV^2 . Moreover, a form factor term is introduced for the high- Q^2 suppression effect, $(1 + Q_1^2/W_{\gamma\gamma}^2)^{-2}(1 + Q_2^2/W_{\gamma\gamma}^2)^{-2}$. The systematic uncertainty of the luminosity

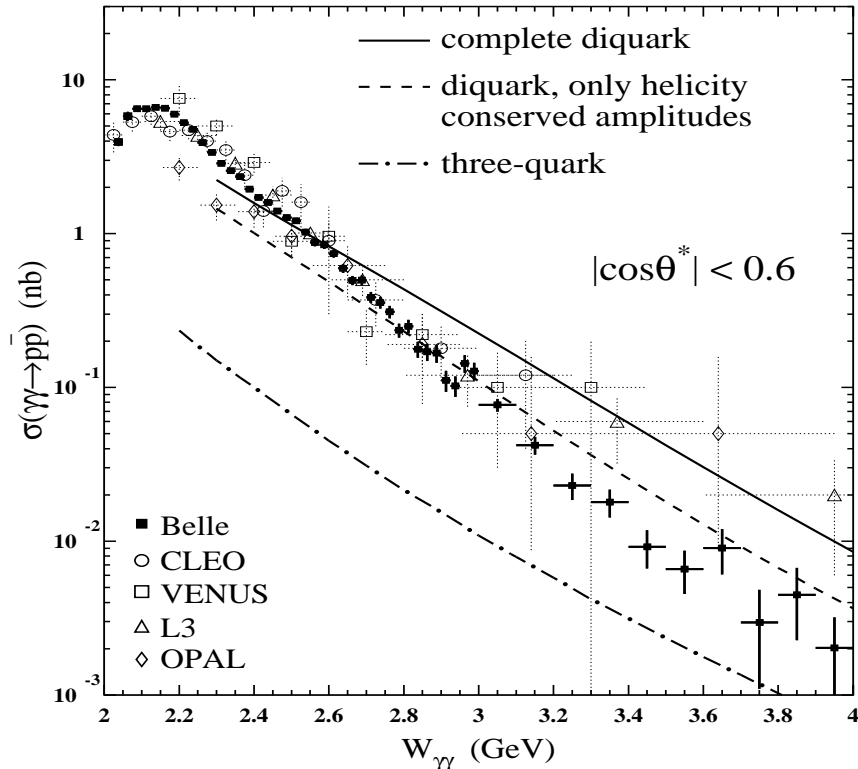


Fig. 4. Measured cross sections for $\gamma\gamma \rightarrow p\bar{p}$. For the Belle, CLEO [8] and VENUS [9] results, the error bars are purely statistical; while for OPAL [10] and L3 [11], both statistical and systematic uncertainties are included. Theoretical prediction curves shown are from [14] (diquark) and [4] (three-quark).

function is estimated by comparing the kinematic distributions of the two-photon system for the events generated with TREPS to those from a QED calculation that includes all order α^4 diagrams [23]. Within the range $W_{\gamma\gamma} = 2 - 4$ GeV agreement within 3 - 5% was reported [22,28].

The cross section $\sigma_{\gamma\gamma \rightarrow p\bar{p}}(W_{\gamma\gamma})$ is obtained by a summation over $|\cos\theta^*|$: $\sum (d\sigma_{\gamma\gamma \rightarrow p\bar{p}}(W_{\gamma\gamma})/d|\cos\theta^*|) \Delta|\cos\theta^*|$, with the restriction of $|\cos\theta^*| < 0.6$, due to polar angular coverage limits of the TOF system. The results are summarized in Table 1 and Fig. 4. The contribution from $\gamma\gamma \rightarrow \eta_c \rightarrow p\bar{p}$ is included in these results. For the two cross section measurements in the lowest $W_{\gamma\gamma}$ bins (2.025 - 2.075 GeV), the efficiencies are extremely small at larger $|\cos\theta^*|$ and data are only available up to $|\cos\theta^*| = 0.4$ and 0.5 , respectively. We thus fit a second-order polynomial function of $\cos^2\theta^*$ to these differential cross sections and arrive at a result by integrating the fit over $|\cos\theta^*|$ up to 0.6. For comparison, we also show in Fig. 4 the results from previous measurements [8,9,10,11].

$W_{\gamma\gamma}$ (GeV)	$\sigma(\gamma\gamma \rightarrow p\bar{p})$ (nb)	$W_{\gamma\gamma}$ (GeV)	$\sigma(\gamma\gamma \rightarrow p\bar{p})$ (nb)
2.025 - 2.050	$3.95 \pm 0.25 \pm 0.28$	2.650 - 2.675	$0.50 \pm 0.03 \pm 0.05$
2.050 - 2.075	$5.79 \pm 0.40 \pm 0.41$	2.675 - 2.700	$0.50 \pm 0.04 \pm 0.05$
2.075 - 2.100	$6.48 \pm 0.29 \pm 0.46$	2.700 - 2.725	$0.39 \pm 0.03 \pm 0.04$
2.100 - 2.125	$6.49 \pm 0.17 \pm 0.49$	2.725 - 2.750	$0.36 \pm 0.03 \pm 0.03$
2.125 - 2.150	$6.64 \pm 0.16 \pm 0.50$	2.750 - 2.775	$0.31 \pm 0.03 \pm 0.03$
2.150 - 2.175	$6.54 \pm 0.14 \pm 0.50$	2.775 - 2.800	$0.24 \pm 0.02 \pm 0.02$
2.175 - 2.200	$5.97 \pm 0.13 \pm 0.47$	2.800 - 2.825	$0.25 \pm 0.03 \pm 0.02$
2.200 - 2.225	$5.26 \pm 0.11 \pm 0.42$	2.825 - 2.850	$0.18 \pm 0.02 \pm 0.02$
2.225 - 2.250	$4.77 \pm 0.10 \pm 0.39$	2.850 - 2.875	$0.17 \pm 0.02 \pm 0.02$
2.250 - 2.275	$3.91 \pm 0.09 \pm 0.32$	2.875 - 2.900	$0.17 \pm 0.02 \pm 0.02$
2.275 - 2.300	$3.38 \pm 0.08 \pm 0.28$	2.900 - 2.925	$0.111 \pm 0.017 \pm 0.010$
2.300 - 2.325	$2.86 \pm 0.07 \pm 0.24$	2.925 - 2.950	$0.101 \pm 0.016 \pm 0.009$
2.325 - 2.350	$2.56 \pm 0.07 \pm 0.22$	2.950 - 2.975	$0.143 \pm 0.019 \pm 0.013$
2.350 - 2.375	$2.34 \pm 0.07 \pm 0.21$	2.975 - 3.000	$0.128 \pm 0.017 \pm 0.011$
2.375 - 2.400	$1.94 \pm 0.06 \pm 0.17$	3.000 - 3.100	$0.077 \pm 0.007 \pm 0.009$
2.400 - 2.425	$1.72 \pm 0.06 \pm 0.16$	3.100 - 3.200	$0.042 \pm 0.006 \pm 0.004$
2.425 - 2.450	$1.59 \pm 0.05 \pm 0.15$	3.200 - 3.300	$0.023 \pm 0.005 \pm 0.002$
2.450 - 2.475	$1.40 \pm 0.05 \pm 0.13$	3.300 - 3.400	$0.018 \pm 0.004 \pm 0.002$
2.475 - 2.500	$1.27 \pm 0.05 \pm 0.12$	3.400 - 3.500	$0.0092 \pm 0.0026 \pm 0.0009$
2.500 - 2.525	$1.21 \pm 0.05 \pm 0.11$	3.500 - 3.600	$0.0066 \pm 0.0021 \pm 0.0007$
2.525 - 2.550	$1.03 \pm 0.05 \pm 0.10$	3.600 - 3.700	$0.0090 \pm 0.0030 \pm 0.0010$
2.550 - 2.575	$0.88 \pm 0.05 \pm 0.08$	3.700 - 3.800	$0.0030 \pm 0.0019 \pm 0.0003$
2.575 - 2.600	$0.84 \pm 0.05 \pm 0.08$	3.800 - 3.900	$0.0045 \pm 0.0022 \pm 0.0005$
2.600 - 2.625	$0.74 \pm 0.04 \pm 0.07$	3.900 - 4.000	$0.0020 \pm 0.0012 \pm 0.0003$
2.625 - 2.650	$0.60 \pm 0.04 \pm 0.06$		

Table 1

Measured cross sections for $\gamma\gamma \rightarrow p\bar{p}$ ($|\cos\theta^*| < 0.6$). The first error is statistical and the second is systematic.

Fig. 5 shows the angular dependence of the differential cross sections measured in 11 ranges of $W_{\gamma\gamma}$ separately. The η_c region (2.9 - 3.1 GeV) is skipped. For $W_{\gamma\gamma} < 2.4$ GeV, the differential cross sections decrease as $|\cos\theta^*|$ increases; while for $W_{\gamma\gamma} > 2.6$ GeV, the opposite trend is observed. The transition occurs around $W_{\gamma\gamma} = 2.5$ GeV. Similar results are shown in Fig. 6 for three larger ranges of $W_{\gamma\gamma}$ and are summarized in Table 2. For comparison, previous measurements [8,10,11] are also shown in Fig. 6. Further discussion is given in Section 6.

Based on studies from Monte Carlo and data, residual backgrounds due to particle misidentification and non-exclusive events are subtracted from the data. Corrections are based on ΔN multiplied by $(1 - f)$ as shown in Eq.(2). Complete details are given in Section 5, and the systematic errors are shown in Table 3. All measured cross sections and differential cross sections shown in this paper have been corrected in this way. The excess caused by the J/ψ background described at the end of Section 2 is estimated in each $|\cos\theta^*|$ bin

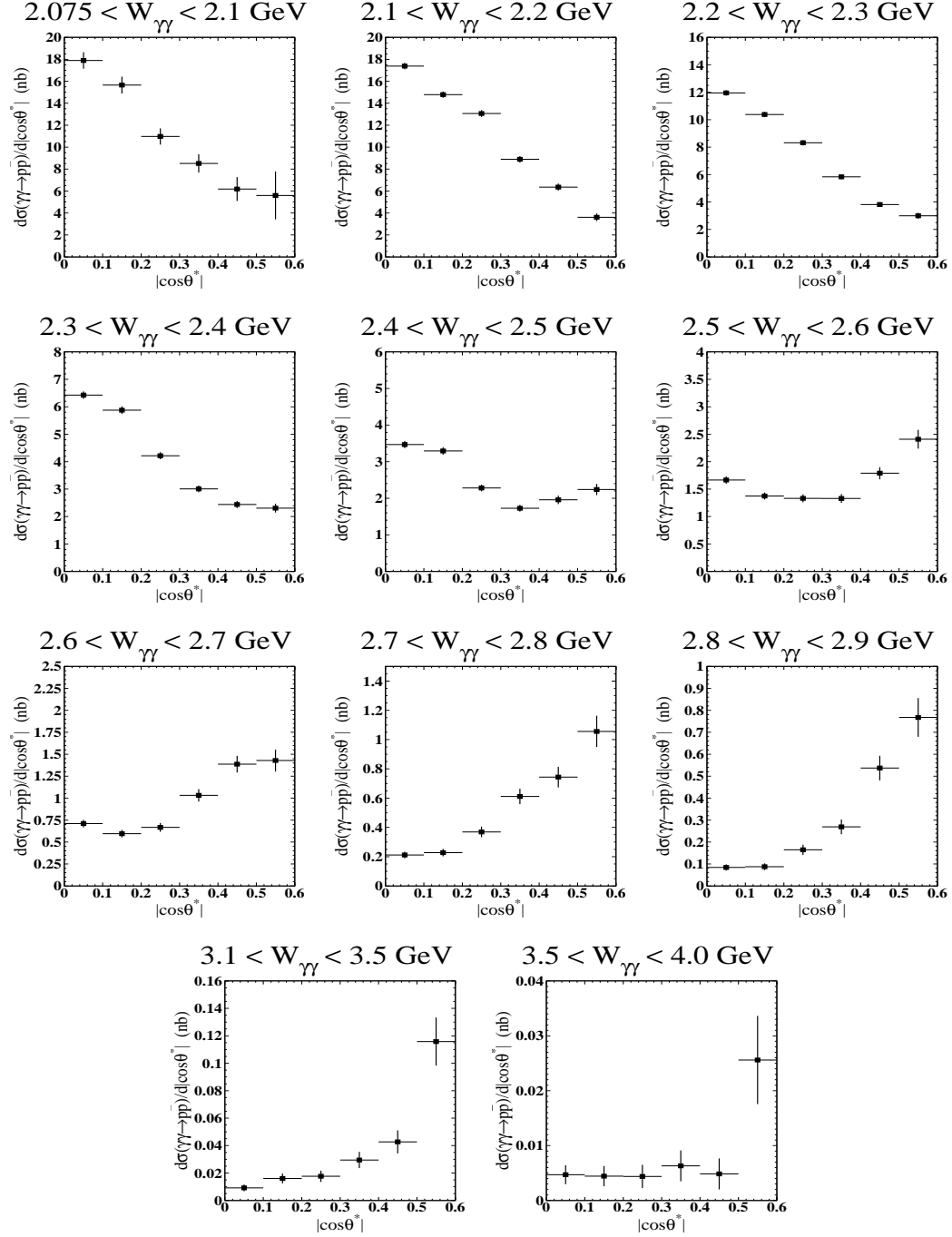


Fig. 5. Measured differential cross sections in 11 ranges of $W_{\gamma\gamma}$ as a function of $|\cos\theta^*|$. The error bars are statistical only.

separately and subtracted from ΔN before the other corrections above. The systematic uncertainty due to this subtraction is 8% for the measured cross section in the 3.0 - 3.1 GeV $W_{\gamma\gamma}$ bin, taking into account the fluctuation of the estimated number of J/ψ .

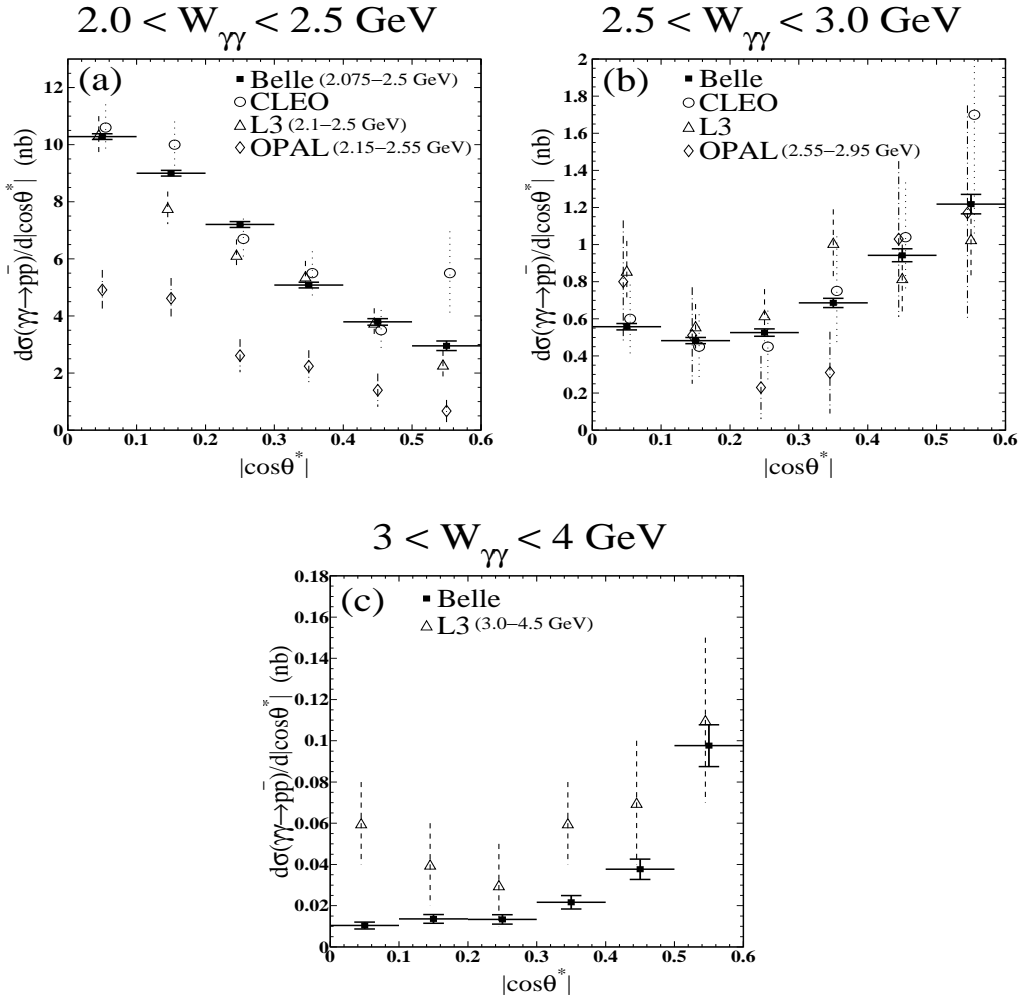


Fig. 6. Measured differential cross sections as a function of $|\cos\theta^*|$ for three ranges of $W_{\gamma\gamma}$. The error bars are statistical only.

$ \cos\theta^* $	$\frac{d\sigma_{\gamma\gamma \rightarrow p\bar{p}}}{d \cos\theta^* }$ (nb) $W_{\gamma\gamma} = 2.075 - 2.5$ GeV	$\frac{d\sigma_{\gamma\gamma \rightarrow p\bar{p}}}{d \cos\theta^* }$ (nb) $W_{\gamma\gamma} = 2.5 - 3.0$ GeV	$\frac{d\sigma_{\gamma\gamma \rightarrow p\bar{p}}}{d \cos\theta^* }$ (nb) $W_{\gamma\gamma} = 3 - 4$ GeV
0.0 - 0.1	$10.28 \pm 0.10 \pm 0.29$	$0.56 \pm 0.02 \pm 0.02$	$0.010 \pm 0.002 \pm 0.002$
0.1 - 0.2	$9.00 \pm 0.10 \pm 0.26$	$0.48 \pm 0.02 \pm 0.02$	$0.014 \pm 0.002 \pm 0.001$
0.2 - 0.3	$7.20 \pm 0.10 \pm 0.27$	$0.53 \pm 0.02 \pm 0.04$	$0.013 \pm 0.002 \pm 0.001$
0.3 - 0.4	$5.08 \pm 0.10 \pm 0.19$	$0.69 \pm 0.03 \pm 0.05$	$0.022 \pm 0.003 \pm 0.002$
0.4 - 0.5	$3.79 \pm 0.12 \pm 0.17$	$0.94 \pm 0.04 \pm 0.03$	$0.038 \pm 0.005 \pm 0.003$
0.5 - 0.6	$2.96 \pm 0.17 \pm 0.13$	$1.22 \pm 0.05 \pm 0.04$	$0.098 \pm 0.010 \pm 0.007$

Table 2

Measured differential cross sections versus $|\cos\theta^*|$ for different $W_{\gamma\gamma}$ ranges. The first error is statistical and the second is systematic.

Source	Systematic error (%)
Integrated luminosity	1.4
Luminosity function	3 - 5
Trigger efficiency	5
Particle identification efficiency	1 - 6
Monte Carlo statistics	1 - 3
Particle misidentification background subtraction	0 - 1
Non-exclusive ($p\bar{p}\pi^0$) background subtraction	2 - 12
$ \Sigma p_t^* $ effect and residual non-exclusive backgrounds	2 - 3
J/ψ subtraction ($W_{\gamma\gamma} = 3.0 - 3.1$ GeV)	8
Possible backgrounds from radiative return	1
Total	7 - 14

Table 3

Systematic errors for the measured cross sections of $\gamma\gamma \rightarrow p\bar{p}$. Some uncertainties are $W_{\gamma\gamma}$ -dependent and shown as ranges.

The total η_c yield, $N_{\eta_c} = 156.9 \pm 33.3$, can be converted to the product of the two-photon width of η_c and the branching fraction of $\eta_c \rightarrow p\bar{p}$: $\Gamma_{\gamma\gamma}(\eta_c) \times B(\eta_c \rightarrow p\bar{p}) = N_{\eta_c} m_{\eta_c}^2 / (4\pi^2 \varepsilon L_{\text{int}} \frac{dL_{\gamma\gamma}}{dW_{\gamma\gamma}}) = 7.20 \pm 1.53(\text{stat.})_{-0.75}^{+0.67}(\text{syst.})$ eV, using the luminosity function $dL_{\gamma\gamma}/dW_{\gamma\gamma}$ determined at the energy of the η_c mass (m_{η_c}) and the efficiency ε from Monte Carlo. For the systematic error, effects from the uncertainties of the continuum background shape and the signal width are taken into account, in addition to all other sources listed in Table 3. The above result gives $\Gamma_{\gamma\gamma}(\eta_c) = 5.5 \pm 1.2(\text{stat.})_{-0.6}^{+0.5}(\text{syst.}) \pm 1.7(\text{norm.})$ keV, where the last error comes from the branching fraction $B(\eta_c \rightarrow p\bar{p})$ uncertainty [20]. Since observations of the η_c in the $p\bar{p}$ channel are scarce and suffer from low statistics, current measurements for $B(\eta_c \rightarrow p\bar{p})$ available in Ref. [20] are not very consistent with each other. Our result is the first measurement of $\Gamma_{\gamma\gamma}(\eta_c) \times B(\eta_c \rightarrow p\bar{p})$ in two-photon collisions and, together with the observation of the η_c in $p\bar{p}$ collisions in its $\gamma\gamma$ decay mode [29], will help to decrease the errors on both the η_c two-photon width and branching fraction.

5 Corrections and major sources of systematic error

The accuracy of the Monte Carlo trigger efficiency has been checked from the two-track trigger, which requires at least two CDC tracks with an opening angle larger than 135° , two or more TOF hits as well as the ECL timing signal, using experimental events passing the high energy trigger based on a 1 GeV threshold for an ECL total energy sum [18,30]. The trigger efficiency depends on the average transverse momentum of the two tracks in the laboratory frame, $\bar{p}_t \cong p_t^{\gamma\gamma} \equiv [(W_{\gamma\gamma}/2)^2 - m_p^2]^{1/2} \cdot (1 - |\cos\theta^*|)^{1/2}$, where the latter is the transverse momentum of $p(\bar{p})$ in the $\gamma\gamma$ c.m. frame. We determine the trigger

efficiency as a function of $p_t^{\gamma\gamma}$, since each of the two-dimensional bins in $W_{\gamma\gamma}$ and $|\cos\theta^*|$, where the number of events is measured, is associated with a $p_t^{\gamma\gamma}$ value using the relation above. From the data, the trigger efficiency is 0.83 ± 0.02 at $p_t^{\gamma\gamma} = 0.55$ GeV/ c and 0.95 ± 0.05 at $p_t^{\gamma\gamma} = 0.95$ GeV/ c . Corrections for the Monte Carlo trigger efficiency are implemented according to the data, with a systematic error within 5%.

The accuracy of the PID efficiencies has been checked by comparing Monte Carlo estimates to those based on data. The efficiency associated with each of the four PID conditions (Section 2) is studied, using events passing all selection criteria except the condition in question. The overall PID efficiency is $\sim 92\%$, $\sim 88\%$ and down to $\sim 78\%$ at $W_{\gamma\gamma} = 2, 3$ and 4 GeV respectively, with a systematic error less than 6% in the whole $W_{\gamma\gamma}$ range. The fake rate is $\sim 0.01\%$ - 0.3% for $W_{\gamma\gamma} = 3 - 4$ GeV, respectively.

Monte Carlo studies indicate that the PID requirements are very efficient in rejecting electrons and other relativistic particles, so that events from $\gamma\gamma \rightarrow \pi^+\pi^-, \mu^+\mu^-$ and e^+e^- do not survive the selection, leaving those from $\gamma\gamma \rightarrow K^+K^-$ as the main residual background. From Monte Carlo simulation and the measured cross sections for $\gamma\gamma \rightarrow K^+K^-$ [27,31], the fraction of data that can be attributed to residual K^+K^- background, f_m , is evaluated. Based on Monte Carlo studies, the dependence of f_m on $|\cos\theta^*|$ is negligible and $f_m(W_{\gamma\gamma}) = 0.8 \pm 0.3\%$, $3.2 \pm 0.5\%$ and $7.7 \pm 0.8\%$ at $W_{\gamma\gamma} = 3.2, 3.6$ and 4.0 GeV, respectively. For $W_{\gamma\gamma} < 3.0$ GeV, f_m is negligible. The values of f_m have been checked in the data, using events passing all selection criteria except that on the normalized likelihood, $\lambda_p > 0.8$. The number of signal events that would pass all selection criteria is estimated from the ΔT distribution of one of the two tracks, after requiring the other to satisfy $\lambda_p > 0.8$. The values of f_m inferred in this way are in good agreement with those above. The contribution from this source of background is subtracted from the data, using the expected f_m from the Monte Carlo studies. The systematic uncertainty due to this source is $\sim 1\%$ or less in the whole $W_{\gamma\gamma}$ range.

Possible non-exclusive backgrounds ($p\bar{p}X$), most of them from $\gamma\gamma \rightarrow p\bar{p}\pi^0$ events, have been searched for in the data. Monte Carlo studies show that a high purity sample of such background can be derived from events with larger $|\Sigma p_t^*|$ and smaller $|\Sigma p_t^*(p\bar{p}\pi^0)|$, the latter being the transverse momentum balance of the three particles. By comparing Monte Carlo and data distributions of these parameters we obtain the fraction of the data attributed to this background type, f_n . We find that the dependence of f_n on $|\cos\theta^*|$ is negligible, and it ranges from $5 \pm 2\%$ to $17 \pm 8\%$ for $W_{\gamma\gamma}$ from 2 to 4 GeV, respectively. Corrections are made using the $f_n(W_{\gamma\gamma})$ obtained above, and in total $7 \pm 1\%$ of the selected data are subtracted. The systematic error from this source is 2 - 12% for $W_{\gamma\gamma}$ from 2 to 4 GeV, respectively. The fraction of the data attributed to $\gamma\gamma \rightarrow p\bar{p}\pi^0$ events is also obtained as a function of $|\Sigma p_t^*|$. Before the cor-

rection, a comparison of the $|\Sigma p_t^*|$ distribution between data and Monte Carlo exhibits a total difference of $\sim 9\%$ between the two samples, while it is reduced to less than 3% for any $W_{\gamma\gamma}$ range after the correction (Fig. 7). Since the residual excess in the $|\Sigma p_t^*|$ distribution could be attributed to residual non-exclusive backgrounds and a broader nature of the signal distribution than the Monte Carlo, the systematic uncertainty due to other possible non-exclusive backgrounds is limited to 3% after the correction.

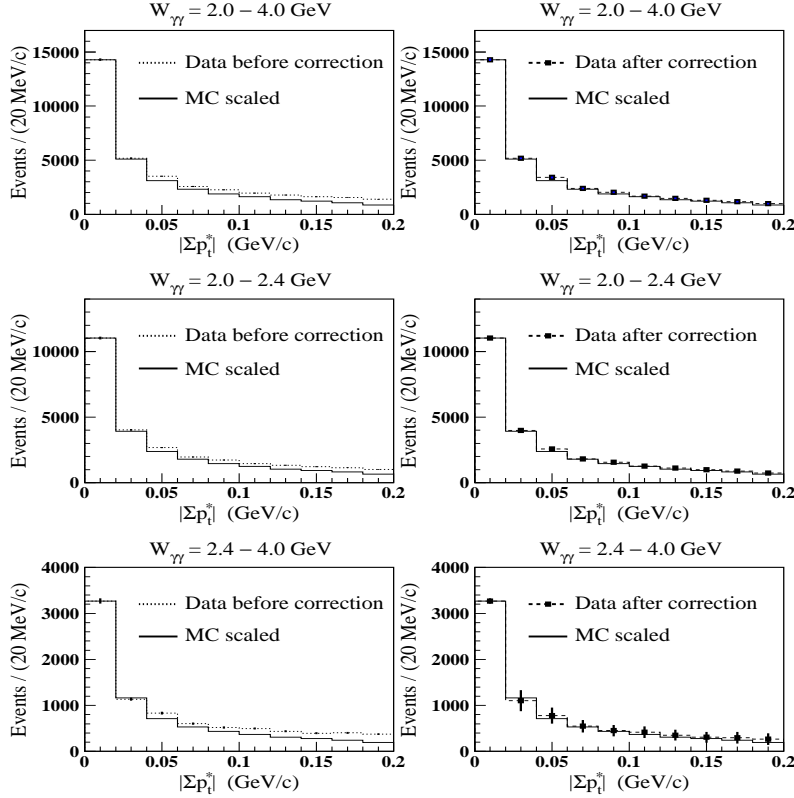


Fig. 7. $|\Sigma p_t^*|$ distributions for the data before (left column) and after (right column) the subtraction of residual non-exclusive backgrounds ($\gamma\gamma \rightarrow p\bar{p}\pi^0$). The Monte Carlo distributions are scaled with the first bin normalized to the data.

6 Theoretical approaches

From the asymptotic QCD prediction of Eq.(1) and after integration over $\cos\theta^*$, the cross section for $\gamma\gamma \rightarrow p\bar{p}$ is proportional to $W_{\gamma\gamma}^{-10}$ for asymptotically large $W_{\gamma\gamma}$. All models based on this framework behave asymptotically as $\sigma \propto W_{\gamma\gamma}^{-10}$. For the diquark scenario, two curves are provided [14]: from the complete diquark model and from the same model with only helicity conserved amplitudes, where p and \bar{p} are in opposite helicity states. The scale of the diquark predictions matches the data for $W_{\gamma\gamma} = 2.5 - 3.0$ GeV, but the

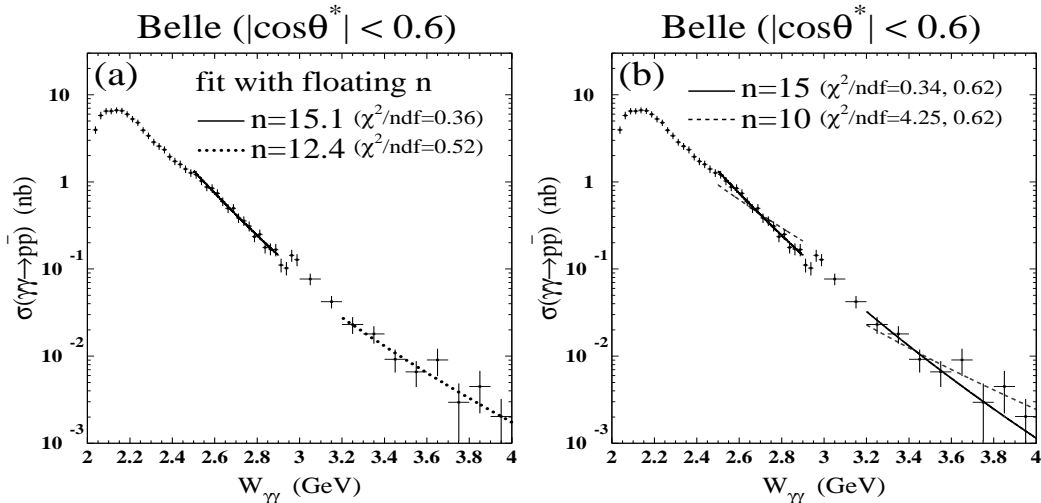


Fig. 8. Separate fits of $\sigma \propto W_{\gamma\gamma}^{-n}$ to the data in the range of $W_{\gamma\gamma} = 2.5 - 2.9$ GeV and $3.2 - 4.0$ GeV, with (a) n floating; (b) $n = 10$ and $n = 15$. The error bars include statistical and systematic errors. The χ^2/ndf values for each fit are indicated in the figure.

deviation becomes larger as $W_{\gamma\gamma}$ increases (Fig. 4). At higher energies, the data fall below the diquark predictions and exhibit a gradual approach to the three-quark model predictions [4]. At medium energies between 2.5 and 4.0 GeV, a steeper fall of the total cross section in $W_{\gamma\gamma}$ is observed.

If we fit the data with a power law $\sigma \propto W_{\gamma\gamma}^{-n}$ with n floating (Fig. 8(a)), taking into account both statistical and systematic uncertainties as well as possible correlations between the latter, we obtain $n = 15.1^{+0.8}_{-1.1}$ and $12.4^{+2.4}_{-2.3}$ in the range of $W_{\gamma\gamma} = 2.5 - 2.9$ GeV and $3.2 - 4.0$ GeV, respectively (the charmonium region between 2.9 and 3.2 GeV is excluded). For completeness, we also show in Fig. 8(b) the results of the fits with n fixed at 10 and 15. Although for both ranges a good fit to the data can be obtained at $n = 15$, a smaller power, $n = 10$, describes the data above 3.2 GeV reasonably well. This may imply that lower power terms become dominant at higher energies, which is an indication for the transition to the asymptotic predictions.

The angular differential cross section in $|\cos\theta^*|$ is another observable most important to the study of the nature of the interactions involved in the process $\gamma\gamma \rightarrow p\bar{p}$. All existing models based on the constituent scattering picture [4,5,12,13,14,15], as expected, predict an ascending trend, which is in agreement with the data for $W_{\gamma\gamma} > 2.5$ GeV. This is due to the factor $1/\sqrt{tu} \propto 1/\sqrt{1 - \cos^2\theta^*}$ contained in the hard scattering amplitudes. The same trend is obtained from naive QED [32] estimates: $d\sigma/d|\cos\theta^*| \propto (1 + \cos^2\theta^*)/(1 - \cos^2\theta^*)$, in the massless limit. A simplified picture with diquarks would follow the naive QED expectation above [10,12], if all quark masses are neglected and only scalar diquarks are considered. In Fig. 9 we plot

the differential cross section normalized to that averaged within $|\cos\theta^*| < 0.3$, and compare various predictions to the data. We observe that the data rise more sharply in $|\cos\theta^*|$ at higher energy (see also Fig. 5). In comparison, all current models predict a flatter trend in $|\cos\theta^*|$.

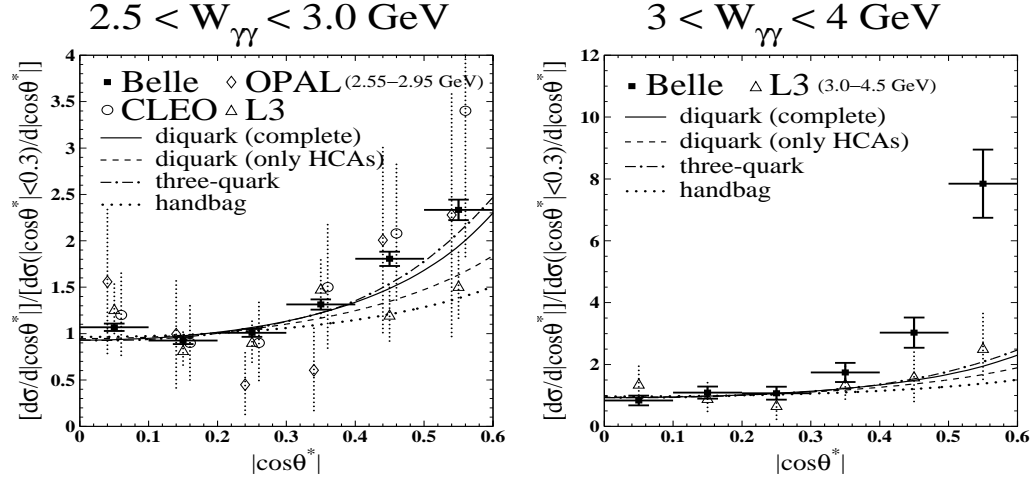


Fig. 9. Differential cross section as a function of $|\cos\theta^*|$, normalized to that averaged within $|\cos\theta^*| < 0.3$, for the two higher ranges of $W_{\gamma\gamma}$. The error bars are statistical only. Theoretical predictions are from [14] (diquark), [5] (three-quark) and [15] (handbag).

The deviation of the leading term QCD calculations [4,5] from the data at $W_{\gamma\gamma} = 2.5 - 4.0$ GeV implies that power corrections are still significant at these intermediate energies. It is not surprising since the very threshold of $p\bar{p}$ production corresponds to $W_{\gamma\gamma} \sim 2$ GeV. However, the diquark and handbag models [12,13,14,15] were developed in order to describe the intermediate energy region at the price of introducing model form factors, *etc.*. The disagreement of the data at $W_{\gamma\gamma} = 2.5 - 4.0$ GeV with their predictions (see Fig. 4 and 9) obviously necessitates their improvement.

The descending trend of the differential cross section in $|\cos\theta^*|$ observed at low energies ($W_{\gamma\gamma} < 2.5$ GeV) cannot be understood within the hard scattering picture (Fig. 6(a)). In a recent study based on non-perturbative QCD sum rules [33], this trend was proposed as a general feature for hadron pair production from two-photon collisions. The behavior is very natural if low partial waves are involved. In Ref. [16] it was shown that even a simple model based on pole- and resonance-dynamics can reproduce this behavior.

7 Conclusion

Using the Belle detector at the high-luminosity KEKB collider, the cross sections for $\gamma\gamma \rightarrow p\bar{p}$ have been measured for $W_{\gamma\gamma}$ from 2.025 to 4.0 GeV and $|\cos\theta^*| < 0.6$, with systematic uncertainties ranging from 7% to 14%. These results represent a great improvement in precision compared to all previous measurements and allow more accurate tests of various theoretical models. We also observed the production of $\gamma\gamma \rightarrow \eta_c \rightarrow p\bar{p}$ and determined the product of the two-photon width of the η_c and its branching ratio to $p\bar{p}$.

Fitting to a power law $\sigma \propto W_{\gamma\gamma}^{-n}$ shows that the best fit value of n decreases as energy increases, and $n = 10$ cannot be rejected at energies above 3.2 GeV, implying the gradual transition to the expectation from asymptotic predictions. The ascending trend for the differential cross section in $|\cos\theta^*|$ predicted by the hard scattering picture is in agreement with the data for $W_{\gamma\gamma} > 2.5$ GeV; however, the data rise more sharply in $|\cos\theta^*|$ as $W_{\gamma\gamma}$ increases. The descending trend in $|\cos\theta^*|$ at lower energies $W_{\gamma\gamma} < 2.5$ GeV can be reproduced by non-perturbative approaches [16]. The descending trend of the differential cross section in $|\cos\theta^*|$ changes to an ascending one with the increase of energy, which could be an indication for the transition from a soft resonance regime to the beginning of a hard regime. Existing models suggested for the intermediate energies [12,13,14,15] can not provide satisfactory description of the observed energy and angular dependence in the studied energy range.

Acknowledgements

We thank the KEKB group for the excellent operation of the accelerator, the KEK cryogenics group for the efficient operation of the solenoid, and the KEK computer group and the NII for valuable computing and Super-SINET network support. We thank C. F. Berger, V. L. Chernyak, H.-N. Li and K. Odagiri for fruitful discussions. We acknowledge support from MEXT and JSPS (Japan); ARC and DEST (Australia); NSFC (contract No. 10175071, China); DST (India); the BK21 program of MOEHRD and the CHEP SRC program of KOSEF (Korea); KBN (contract No. 2P03B 01324, Poland); MIST (Russia); MESS (Slovenia); SNSF (Switzerland); NSC (under Grant No. NSC-92-2112-M-008-028) and MOE (Taiwan); and DOE (USA).

References

- [1] V. L. Chernyak and A. R. Zhitnitsky, JETP Lett. 25 (1977) 510 (Pis'ma v ZhETF 25 (1977) 544); V. L. Chernyak, V. G. Serbo, A. R. Zhitnitsky, JETP Lett. 26 (1977) 594 (Pis'ma v ZhETF 26 (1977) 760).
- [2] G. P. Lepage and S. J. Brodsky, Phys. Lett. B 87 (1979) 359; G. P. Lepage and S. J. Brodsky, Phys. Rev. D 22 (1980) 2157.
- [3] V. L. Chernyak and A. R. Zhitnitsky, Phys. Rept. 112 (1984) 173.
- [4] G. R. Farrar, E. Maina and F. Neri, Nucl. Phys. B 259 (1985) 702.
- [5] G. R. Farrar et al., Nucl. Phys. B 311 (1989) 585.
- [6] V. L. Chernyak and I. R. Zhitnitsky, Nucl. Phys. B 246 (1984) 52.
- [7] M. Althoff et al. (TASSO Collaboration), Phys. Lett. B 130 (1983) 449; W. Bartel et al. (JADE Collaboration), Phys. Lett. B 174 (1986) 350; H. Aihara et al. (TPC/Two-Gamma Collaboration), Phys. Rev. D 36 (1987) 3506; H. Albrecht et al. (ARGUS Collaboration), Z. Phys. C 42 (1989) 543.
- [8] M. Artuso et al. (CLEO Collaboration), Phys. Rev. D 50 (1994) 5484.
- [9] H. Hamasaki et al. (VENUS Collaboration), Phys. Lett. B 407 (1997) 185.
- [10] G. Abbiendi et al. (OPAL Collaboration), Eur. Phys. J. C 28 (2003) 45.
- [11] P. Achard et al. (L3 Collaboration), Phys. Lett. B 571 (2003) 11.
- [12] M. Anselmino, F. Caruso, P. Kroll and W. Schweiger, Int. J. Mod. Phys. A 4 (1989) 5213.
- [13] P. Kroll, Th. Pilsner, M. Schürmann and W. Schweiger, Phys. Lett. B 316 (1993) 546.
- [14] C. F. Berger and W. Schweiger, Eur. Phys. J. C 28 (2003) 249.
- [15] M. Diehl, P. Kroll and C. Vogt, Eur. Phys. J. C 26 (2003) 567.
- [16] K. Odagiri, Nucl. Phys. A 748 (2005) 168.
- [17] M. Ambrogiani et al. (Fermilab E835 Collaboration), Phys. Rev. D 62 (2000) 052002.
- [18] A. Abashian et al. (Belle Collaboration), Nucl. Instr. Meth. A 479 (2002) 117.
- [19] S. Kurokawa and E. Kikutani, Nucl. Instr. Meth. A 499 (2003) 1.
- [20] S. Eidelman et al. (Particle Data Group), Phys. Lett. B 592 (2004) 1.
- [21] V. M. Budnev, I. F. Ginzburg, G. V. Meledin and V. G. Serbo, Phys. Rep. 15 (1974) 182.
- [22] S. Uehara, KEK Report 96-11 (1996).

- [23] F. A. Berends, P. H. Daverveldt and R. Kleiss, *Comp., Phys. Comm.* 40 (1986) 285.
- [24] egpc v207, L3 program library, 1999, converted for the Belle configuration by S. Hou, 2000.
- [25] R. Brun et al., CERN DD/EE/84-1 (1987).
- [26] J. H. Boyer et al. (Mark II Collaboration), *Phys. Rev. D* 42 (1990) 1350; H. J. Behrend et al. (CELLO Collaboration), *Z. Phys. C* 56 (1992) 381; F. Yabuki et al. (VENUS Collaboration), *Jour. Phys. Soc. Jpn.* 64 (1995) 435.
- [27] H. Nakazawa et al. (Belle Collaboration), hep-ex/0412058.
- [28] K. Abe et al. (Belle Collaboration), *Phys. Lett. B* 540 (2002) 33.
- [29] C. Baglin et al., *Phys. Lett. B* 187 (1987) 191; T. A. Armstrong et al., *Phys. Rev. D* 52 (1995) 4839; M. Ambrogiani et al., *Phys. Lett. B* 566 (2003) 45.
- [30] B. G. Cheon et al., *Nucl. Instr. Meth. A* 494 (2002) 548.
- [31] K. Abe et al. (Belle Collaboration), *Eur. Phys. J. C* 32 (2004) 323.
- [32] F. M. Renard, *Basics of electron positron collisions*, Editions Frontières, 1981.
- [33] R.-C. Hsieh and H.-N. Li, *Phys. Rev. D* 70 (2004) 056002.